Comprehensive Characterization of Electrostatically-Actuated Beams

E. K. Chan, K. Garikipati, and R. W. Dutton

CISX 305, Center for Integrated Systems

Stanford University

Stanford, CA 94305-4075

Email: edward_chan@alumni.stanford.org

Tel: (650) 723-1482 Fax: (650) 725-7731

Abstract

The entire process of calibrating an electromechanical simulator – identifying relevant parameters, designing and measuring test structures, extracting parameters using detailed electromechanical simulations, and extrapolating the behavior of an actual device – is presented. The simulation model for electrostatically-actuated beams is calibrated to a wide range of electrical and optical test structure measurements and is then used to predict the behavior of more complex dual-bias-electrode structures. Various mechanical discontinuities, and post-buckled pull-in behavior are addressed explicitly. Arbitrary fitting coefficients that limit generality are avoided. The well-characterized behavior of the dual-electrode structures can serve as verification test cases for evaluating coupled electromechanical simulators.

1. Introduction

Computer simulation tools such as Abaqus [1][2], IntelliCAD [3] and MEMCAD [4] are being used increasingly to design and understand the behavior of complex electromechanical devices. These tools need to be thoroughly calibrated to particular fabrication processes in order to produce useful and accurate results. Researchers have been measuring resonant frequencies [5], observing the effects of stress on rotating or buckling structures [6][11][13], probing beams with mechanical profilers [7], measuring displacements under electrostatic forces [8][12], and performing traditional uniaxial tensile tests [9] to determine material properties. The reported properties vary considerably for a given material, even for the polysilicon layer in the widely-used Multi-User MEMS Process (MUMPs) of the Microelectronics Center of North Carolina (MCNC) [10]. These variations could be due to errors and approximations in measurements and modeling, or due to actual variations in material properties depending on actuation method, actuation direction, specimen size and sample preparation. Ideally, running a whole battery of parameter extraction methods on test structures on a single die would reveal a consistent set of material parameters. Each method has limited resolution, however, making it difficult to make definitive comparisons or to determine phenomena such as anisotropy.

This paper unifies two different parameter extraction methods to generate a consistent simulation model calibrated to the MUMPs process. The simulation model is calibrated to optical (buckling amplitude) and electrical (pull-in voltage) measurements concurrently, not independently as in [11] and [12], thus increasing confidence in the extracted parameters. A simulation-based model consisting of geometrical and material

property information precludes the need for rather ad hoc parametric adjustments and simplifying assumptions [12][13]. The calibration steps shown in Fig. 1 consist of identifying relevant simulation model parameters, designing suitable test structures, extracting parameters using detailed yet fast electromechanical simulations, and finally extrapolating the behavior of an actual complex device. This paper targets electrostatically-actuated beams fabricated in the POLY1 layer although the extracted

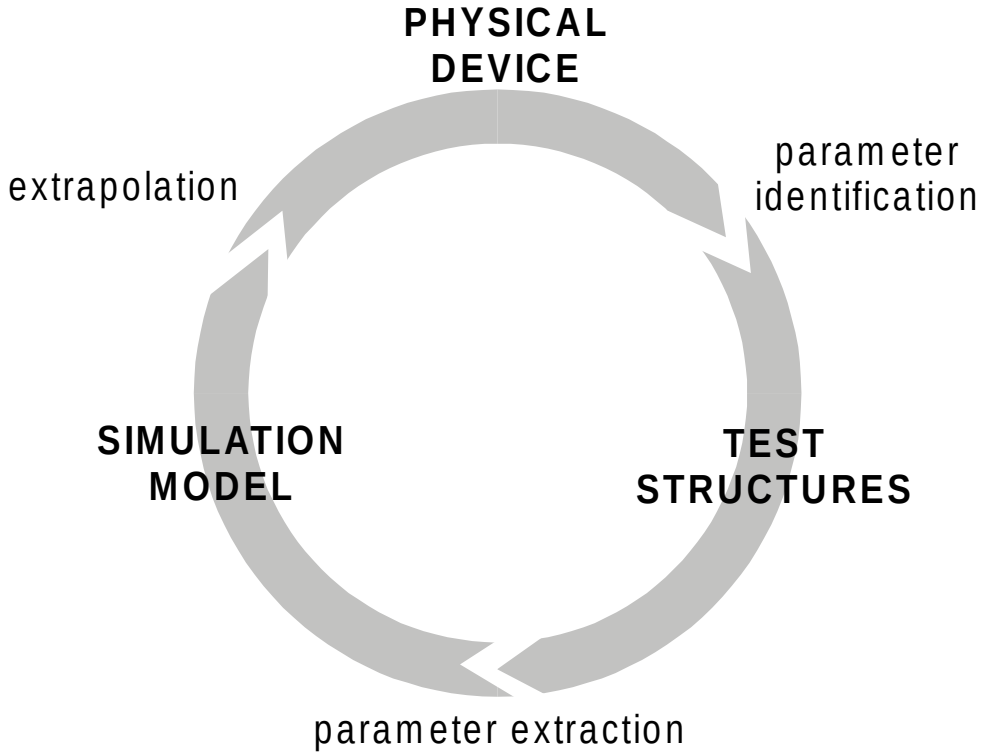

Fig. 1. *Simulator calibration steps for accurate simulation results.*

properties can be used to simulate other devices. However, one must be cautious whenever simulating different modes of actuation or regimes of operation, or devices with dimensions beyond the range of the calibration. Uniformity of material properties cannot always be extrapolated.

In the text that follows, the MUMPs system of materials used to fabricate electrostatically-actuated beams is described, highlighting the effects of overetch, the

observed variations among beams of different width, and the influences of gold pads. The simulation model in Abaqus is then described, emphasizing geometric accuracy at steps. Basic measurement techniques are introduced before the calibration of flat beams to pull-in voltages and buckling amplitudes is explained. The observed transition in pull-in behavior of post-buckled beams beyond a threshold length is detailed. The calibration steps are then repeated for beams with steps over underlying POLY0 pads, and beams with dimples. Beams with dimples buckle downwards instead of upwards and as a result do not exhibit the three regions of pull-in behavior as in the cases of flat beams and beams over POLY0. The well-characterized Abaqus simulation model is then extended to predict the behavior of dual-bias-electrode structures. The extrapolation is very good, verifying the accuracy of the calibration methodology. Hence, the behavior of the dual-bias-electrode devices along with the extracted parameters can serve as benchmark verification cases for evaluating coupled electromechanical simulators. Finally, 3D IntelliCAD simulations are shown for comparison.

2. Material System

2.1 Fabrication overview

Fig. 2 shows the cross-section of an electrostatically-actuated beam fabricated in the MUMPs process. The vertical (height) dimension is greatly exaggerated here and in most of the other figures. In this surface micromachining process, a 0.6μm film of silicon nitride is first deposited on a heavily-doped silicon substrate. The nitride serves as a dielectric isolation layer. The first layer of polysilicon, a 0.5μm-thick layer of POLY0, is then deposited on the nitride and patterned using Reactive Ion Etching (RIE).

This patterning step also thins down exposed areas of silicon nitride. 2μm of sacrificial phosphosilicate glass (PSG) is put down next. Portions of the PSG are then etched through so that polysilicon deposited later can be anchored to the nitride or POLY0

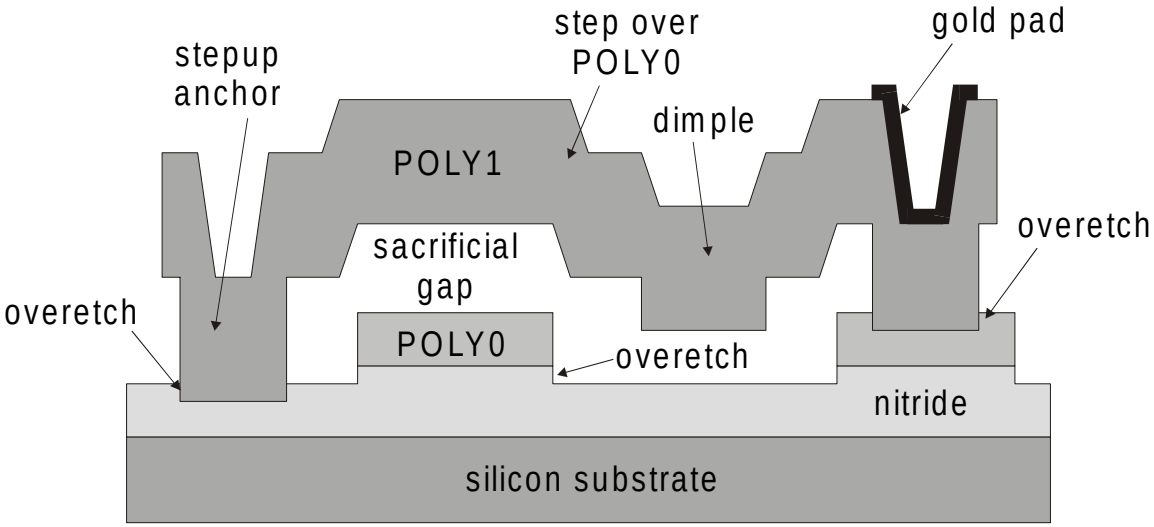

Fig. 2. *Profile of typical electrostatically-actuated structure fabricated in MUMPs showing discontinuities and effects of overetch.*

layers. This anchor etch overetches about 0.13μm of nitride and about 0.02μm of POLY0. A shorter, well-controlled PSG etch of about 0.75μm creates dimples. The main structural layer, 2μm of polysilicon (POLY1), is then deposited and patterned. In addition to the stepup anchors, the conformal polysilicon layer can have steps over POLY0 pads, and steps down into dimples which affect beam behavior. Another sacrificial and another structural layer are deposited and patterned after this but are not shown in Fig. 2. Gold is the final layer, deposited for probing and electrical routing. At the end, the sacrificial PSG is etched away in an HF solution releasing the POLY1 layer leaving freestanding beams anchored to the nitride or POLY0. An electrochemical potential set up during this wet release step results in uneven overetching of the polysilicon layers causing effects described later in this paper.

Measurements in this paper were made on a single die on the MUMPs27 run unless noted otherwise. The die was supercritically dried after a 2.5 minute HF release to obtain long freestanding beams. Rather than trying to extract parameters in light of run-to-run or even die-to-die variations, the goal of this paper is to come up with very accurate geometric and material properties, and hence to validate two consistent parameter extraction methodologies and their underlying coupled electromechanical simulation model.

2.2 Thicknesses

The geometric properties of interest are the thicknesses of the POLY0, POLY1, nitride and sacrificial PSG layers, the depth of the dimple, and the shape of the stepup anchors and other steps. The electrical thickness of the nitride is determined from capacitance measurements. This thickness is an upper bound since the nitride that is not under POLY0 is thinned down during the POLY0 and PSG etches. The thickness of the POLY1 layer is measured at the base of a stepup anchor deposited on POLY0 as shown in the Scanning Electron Micrograph (SEM) of Fig. 3. The error in this measurement, made using a Zygo NewView 200 white light interferometer with a repeatable precision of about 0.01μm, is defined as the difference between the measured value and the actual thickness of a freestanding POLY1 beam. The overetch of about 0.02μm [14] of the underlying POLY0 pad during the anchor etch causes the measured thickness to be slightly less than the actual thickness. This discrepancy is offset in part by the overetch of the underside of an actual freestanding beam during the HF release, and by surface roughness which adds to optical thickness measurements but not to structural rigidity. An alternate measurement is the height of a released POLY1 beam pegged to a POLY0

layer. This measurement, however, includes the effects of surface residue which can be significant. The POLY1 thickness along with all the other dimensions used in subsequent simulations are shown in Table 1.

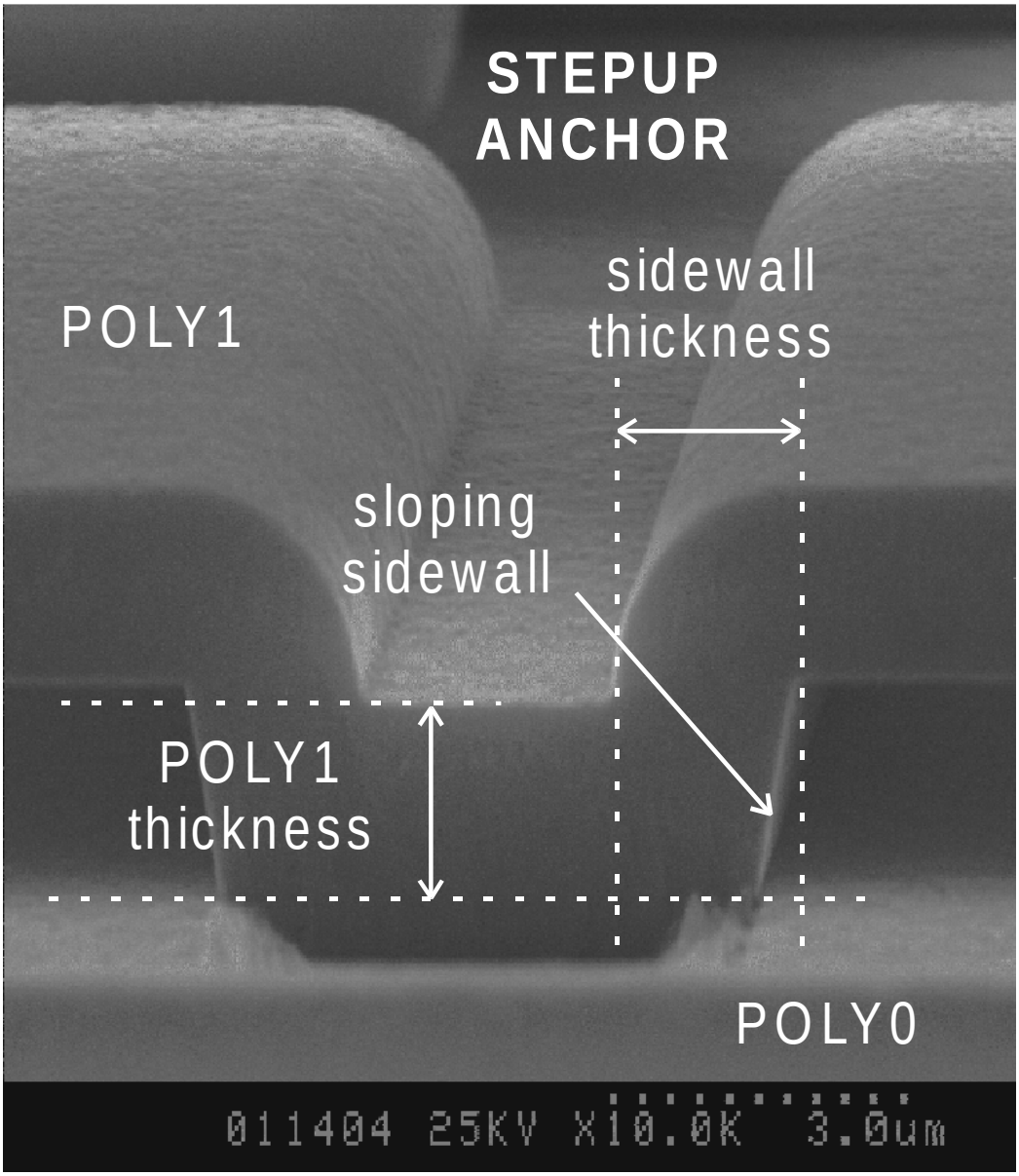

Fig. 3. *SEM of stepup anchor showing thickness measurement site, and sidewall geometry.*

The thickness of the POLY0 layer is measured with respect to the exposed nitride surface thus including the nitride overetch as shown in Fig. 2. The sacrificial gap is

determined by subtracting the thickness of the POLY1 layer from the height of an unreleased POLY1-plus-PSG stack deposited on POLY0. Interferometric measurements show that POLY0 layers connected to gold bonding pads are about 0.01μm thinner, and have rougher surfaces and hence lower reflectivity than isolated POLY0 layers. This

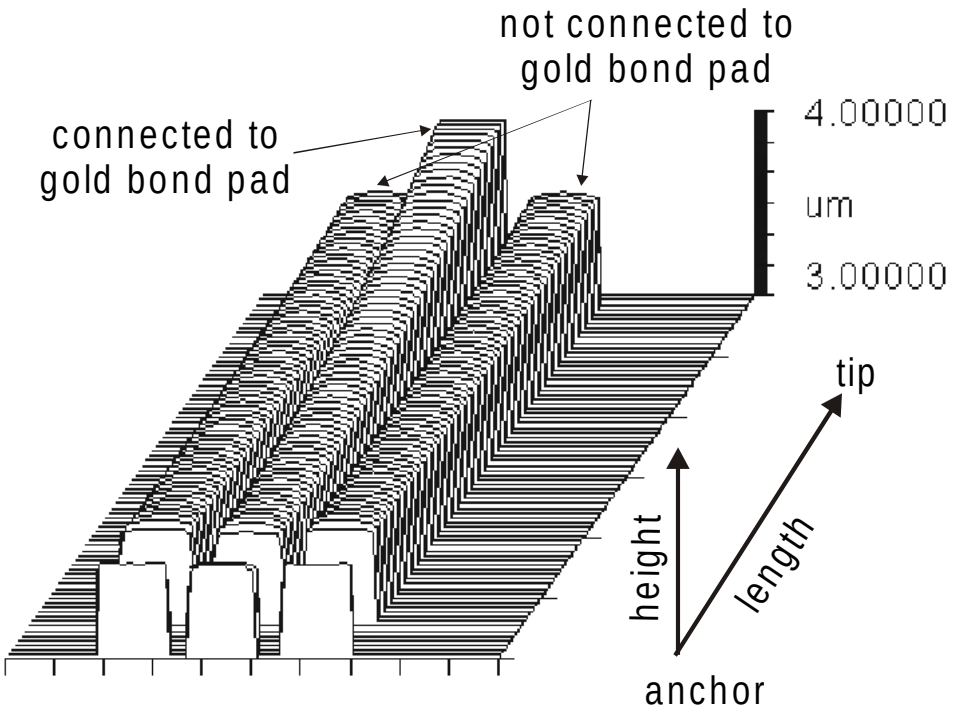

Fig. 4a. *Interferometric image of three unloaded, freestanding POLY1 cantilevers with similar designs except that the center one is connected to a gold bond pad. The center cantilever curls up more. Interferometric images only show top surfaces therefore the sacrificial gap is not displayed. The beams are 300μm long and anchored to the nitride layer. Height is referenced to POLY0 layer.*

might be due to an electrochemical potential set up by the gold pads that increases the etch rate of the POLY0 layer during the HF release etch. The influence of a gold pad depends on the amount of exposed surface area of the polysilicon part that it is connected to. This slight etching of the POLY0 layer causes the sacrificial gap between the nitride and POLY1 to be about 0.01μm less than the gap between the POLY0 and POLY1. It is difficult to accurately determine how the thicknesses of the POLY1 layers are affected although other effects of gold are visible in Figs. 4a and 4b. Three similarly designed

POLY1 cantilevers are shown in Fig. 4a with the only difference being that the center cantilever is connected to a gold pad. That center cantilever curls up more than the other two cantilevers. In Fig. 4b, the center fixed-fixed beam that is connected to gold buckles 0.62μm higher than the other 700μm beams that are not connected to gold. Thus, the presence of gold induces non-uniformity among ostensibly similar devices. All the polysilicon parts measured in this paper are connected to gold pads unless noted otherwise.

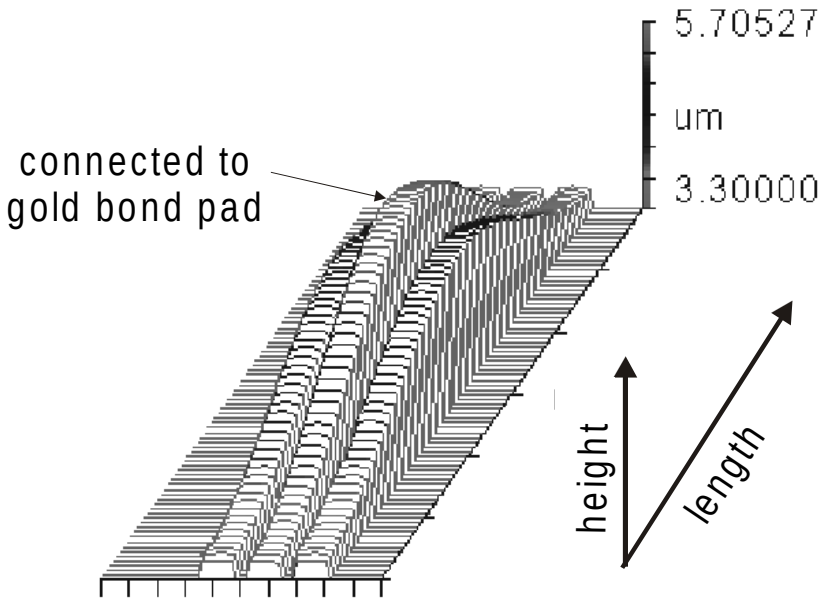

Fig. 4b. *Interferometric image of three POLY1 fixed-fixed beams with similar designs except that the center one is connected to a gold bond pad. The buckling amplitude of the center beam is 0.62μm larger. Interferometric images only show top surfaces therefore the sacrificial gap is not displayed. The beams are 700μm long and anchored to the nitride layer. Height is referenced to POLY0 layer.*

2.3 Dependence on beam width

The behavior of the beams also shows a dependence on their widths. Fig. 5 is an interferometric image of an array of cantilevers of similar length but of varying widths fabricated in MUMPs25. The beams, all without connections to gold, curl down with

different radii of curvature with the exception of the anomalous 10μm-wide beam which actually curls up. The narrower the beams, the more susceptible the beams are to small deviations in the cross-section from an ideal rectangular shape. In addition, each of the beams exhibits variations in height along its width as shown in the cross-sectional profile. The top surfaces of the narrower beams (less than 50μm wide) are rounded. This roundedness is probably due to uneven etching of the surface during the release etch rather than due to bending. Bending in such a deformation mode – widthwise curling

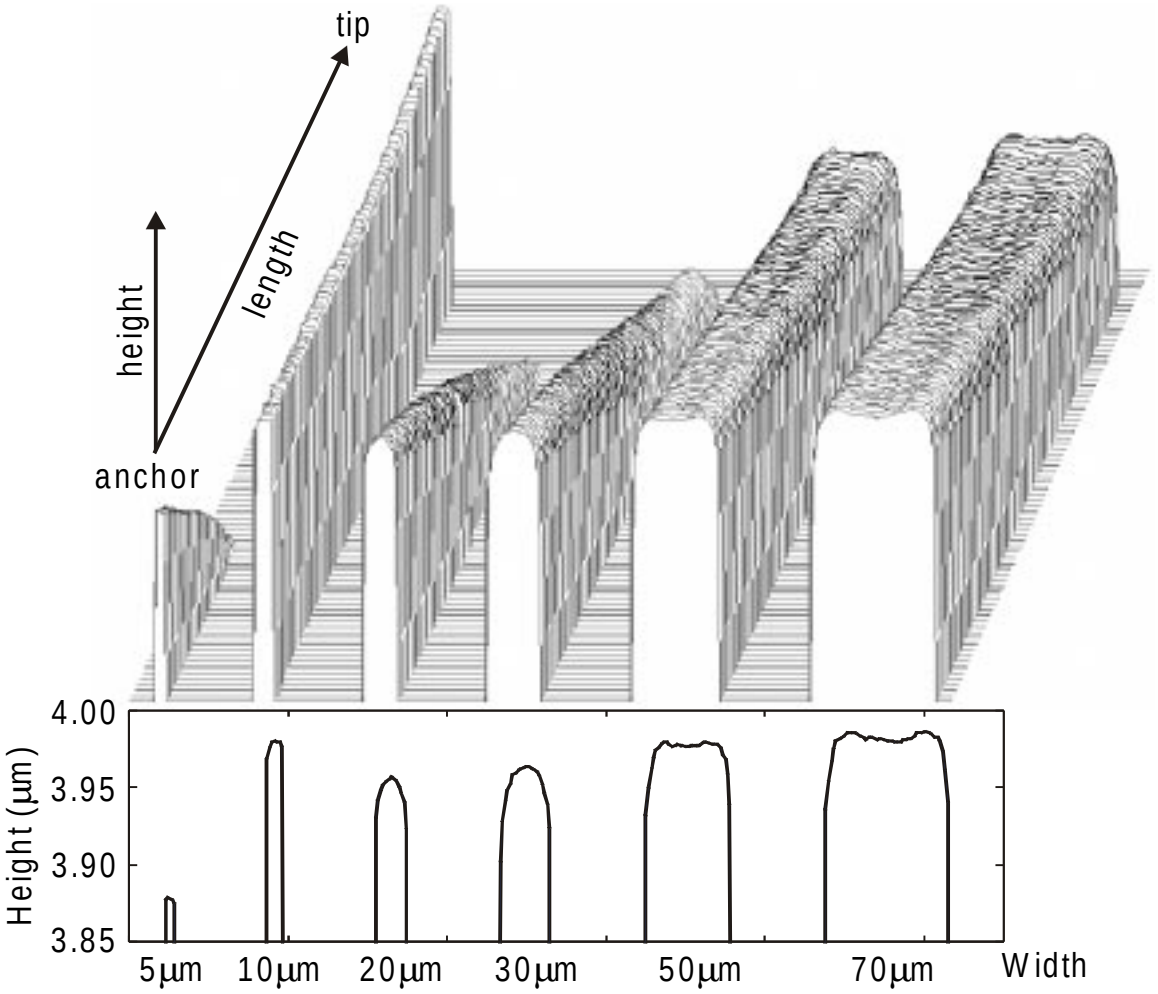

Fig. 5. *Interferometric image of the unloaded deflection of released cantilevers of various widths fabricated in MUMPs 25. The beams exhibit different degress of curvature, and surface height variations along the direction of the width. Beams are anchored to nitride. Height is referenced to POLY0 layer.*

without significant curling along the length – cannot be simulated using isotropic stress gradients. The wider beams show saddle-like height variations along their widths with rounded ridges near each edge. It is possible that the two ridges coalesced into one mound in the case of the narrower beams. Since the source of such widthwise variations

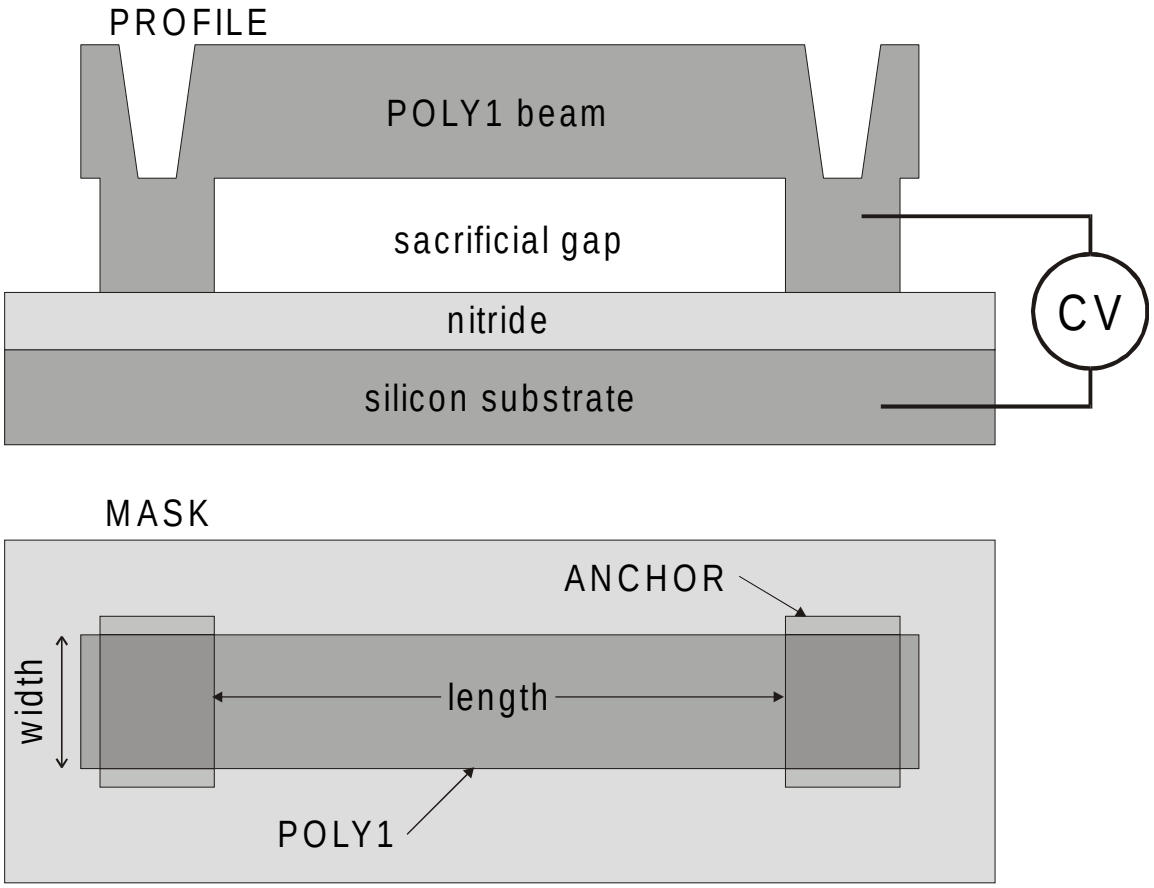

Fig. 6. *Profile and mask design of an electrostatically-actuated beam. Beam is flat except for anchors. Anchors are designed to be essentially two-dimensional without enclosure lips.*

is unclear, only 30μm-wide beams are used for the calibration to minimize the effects of non-ideal cross-sections while avoiding saddle-like height variations. Nonetheless, simulations show that widthwise variations of the observed magnitudes have only minor effects on the pull-in and buckling behavior of the fixed-fixed beams studied here. The characterization of cantilever beams is more involved, however, and requires more study.

Every calibration procedure is necessarily limited to a range of devices and dimensions. This paper examines in detail electrostatically-actuated 30μm-wide POLY1 fixed-fixed beams with stepups and other discontinuities. Geometrical dimensions are first measured then initial biaxial stress and Young's modulus are extracted. The electrical behavior of all layers is assumed ideal with no frequency dependence i.e. the polysilicon layers are perfect conductors, and the sacrificial gap and nitride dielectric are perfect insulators.

3. Calibration to flat beams

3.1 Simulation model

Fig. 6 shows the profile and mask design of an electrostatically-actuated beam, with the top electrode being the POLY1 beam and the lower electrode the silicon substrate. Except for the stepup anchor regions, the beams were fabricated flat. For the best match to simulations, the beams were designed to be essentially two-dimensional without POLY1 enclosure lips around the anchors [2]. The 2D simulation model in Abaqus is shown in Fig. 7 highlighting the geometry of the stepup anchors and other

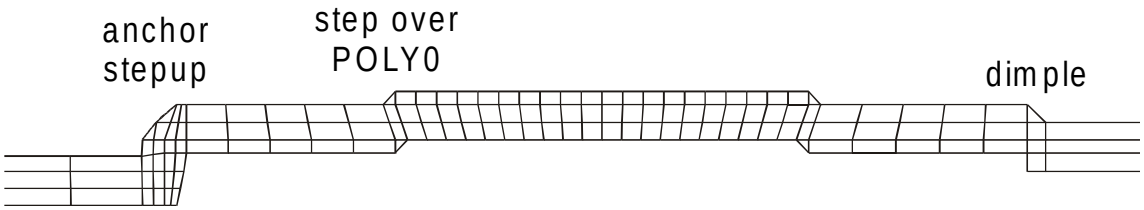

Fig. 7. *Mesh in Abaqus of a portion of the dual-bias electrode structure, capturing the stepup sidewall detail and the effects of overetch. Quadratic reduced-integration plane stress elements are used everywhere except at the anchor where plane strain elements are used.*

mechanical discontinuities which correspond to the SEMs of Figs. 3 and 8. The effects of overetch, sloping sidewalls and conformal deposition are included. Full three-

dimensional (3D) simulations consume enormous computing resources and time, making them infeasible for parameter extraction procedures which require the solutions of many variations of a given system. Electrostatic forces, using parallel-plate approximations

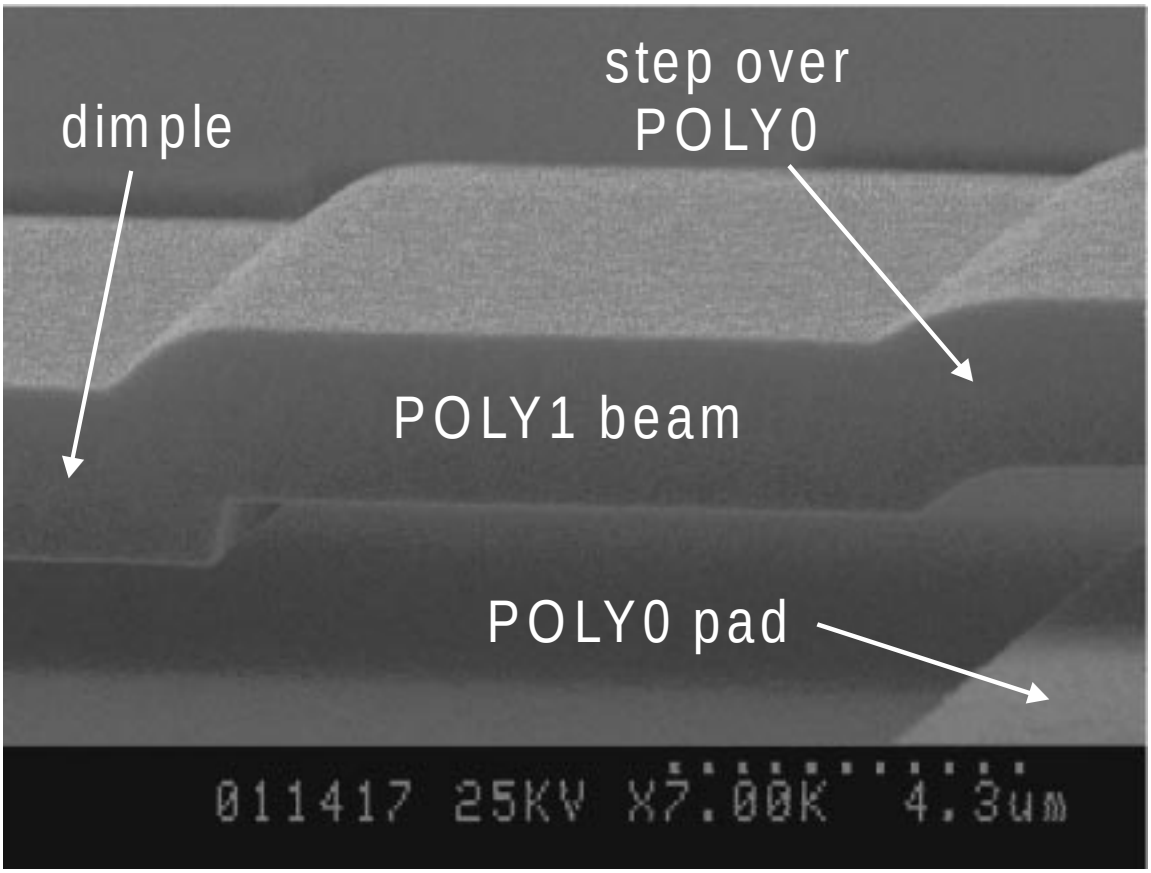

Fig. 8. *SEM of step over POLY0 and step into dimple.*

that account for the effects of fringing fields and finite beam thickness, are incorporated into Abaqus as user-defined loads. A thorough analysis of such 2D coupled electromechanical simulations along with comparisons to full 3D simulations was presented in [2].

3.2 Buckling amplitude

The POLY1 layer in MUMPs is deposited slightly compressive. As a result, beams fabricated in POLY1 tend to deform to relieve some of that stress. Eq. 1 is an analytical expression for the buckling amplitude of fixed-fixed beams

$$u_{\max} = \sqrt{\frac{k\alpha L^2}{\pi^2} - \frac{4}{3}t^2} \tag{1}$$

where k is a constant that depends on boundary conditions, α is the initial (pre-buckled) strain, L is beam length, and t is beam thickness. In contrast to the ideal case where deflection occurs only beyond a threshold buckling beam length, beams with stepup

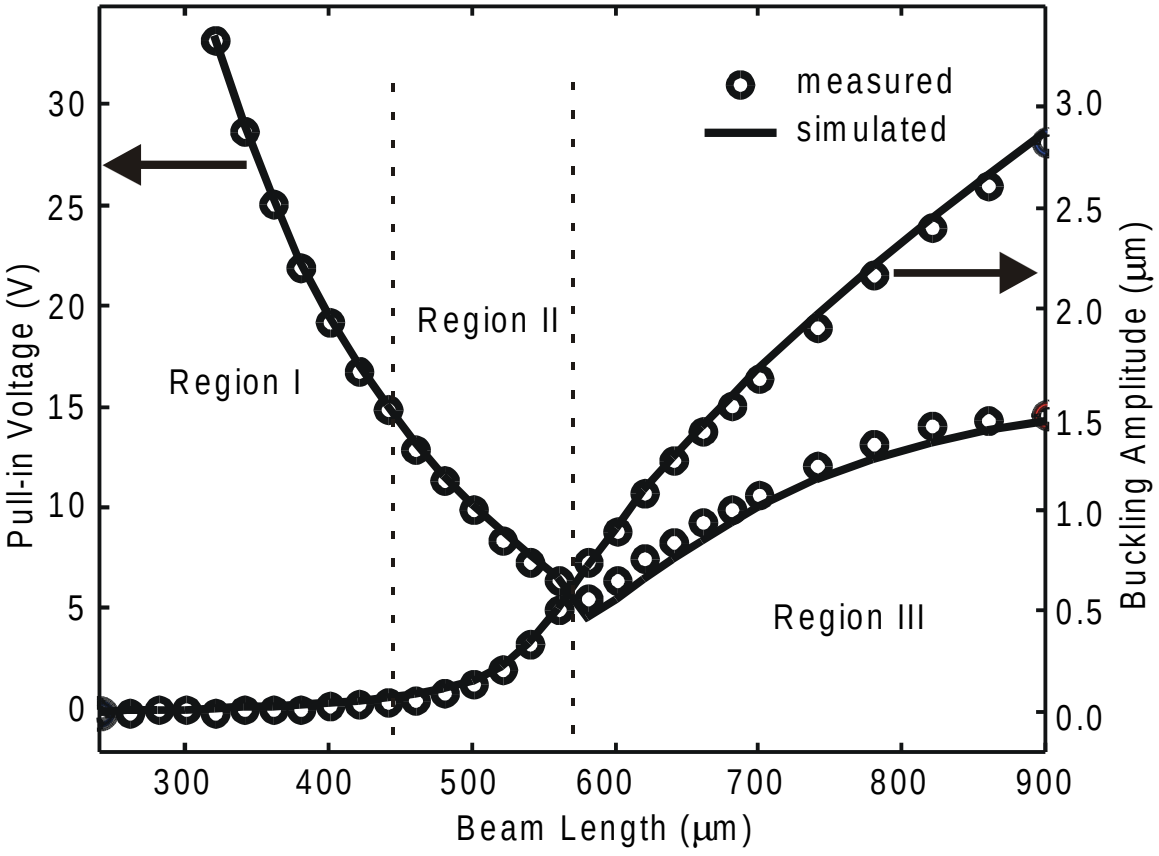

Fig. 9. *Pull-in voltages and buckling amplitude of flat beams as functions of beam length. Three regions of pull-in behavior are demarcated.*

anchors deform even at shorter lengths. This is shown in Fig. 9 where buckling amplitudes along with pull-in voltages are plotted as functions of beam length. The

transition from the pre-buckled state to the post-buckled state is not abrupt. Since the buckling amplitude depends strongly on initial strain but not at all on Young's modulus, the strain parameter can be extracted by fitting Abaqus simulations to the measured buckling amplitudes for various beams. The measurements were made with the Zygo

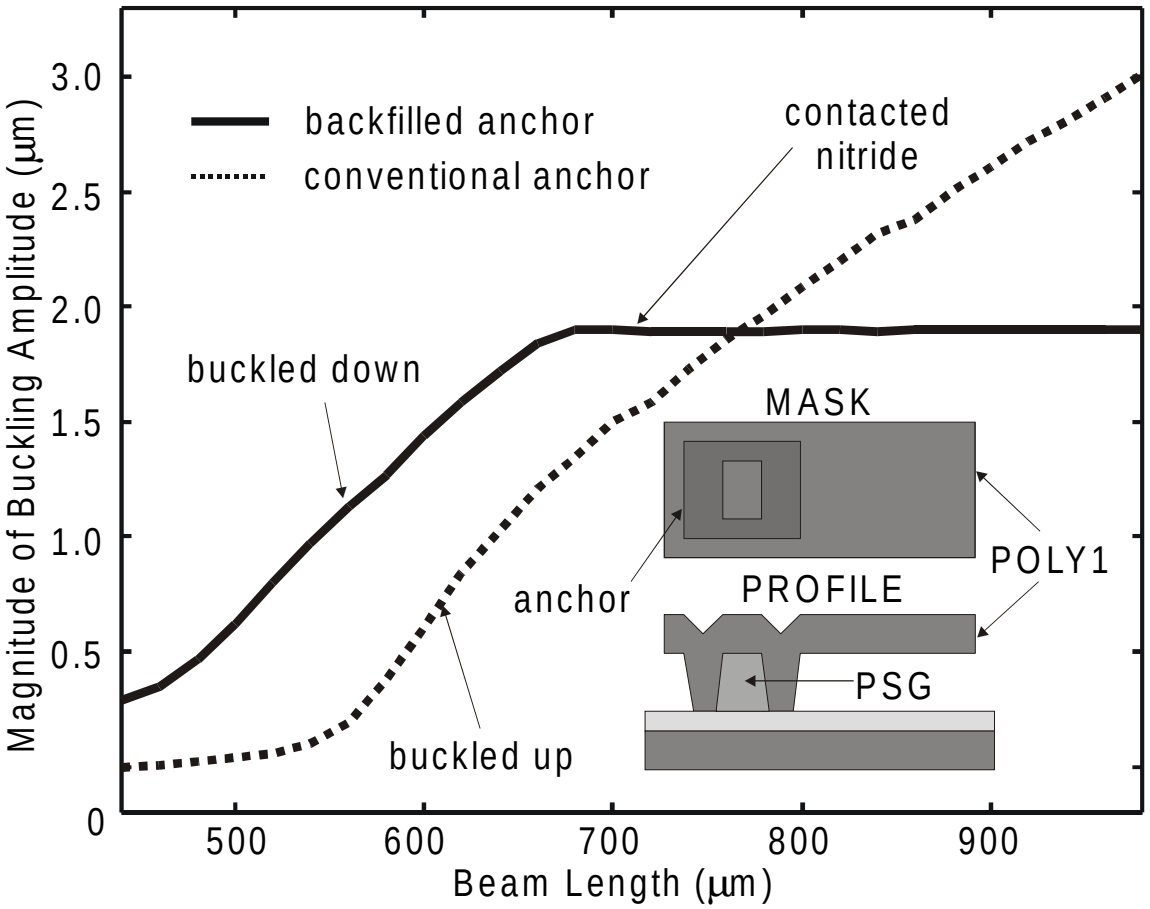

Fig. 10. *Measured magnitude of buckling amplitude for beams with backfilled anchors compared to beams with conventional anchors. Mask design and profile of anchor is shown in inset. Beams were fabricated in MUMPs 25 run.*

interferometer using POLY0 layers instead of the nitride as reference levels to minimize the effects of secondary fringes and poor reflectivity. The excellent fit indicates that the other two parameters critical to buckling amplitude – boundary conditions and beam thickness – are as determined from interferometric measurements and SEMs. Measurements of beams with backfilled stepup anchors [15] show that the pressure due

to encapsulated PSG in such anchors causes the beams to deflect downwards instead of upwards. Furthermore, at any given length, the amplitude of deflection is larger than for beams with conventional stepups as shown in Fig. 10.

3.3 Pull-in voltage

When a voltage is applied between the beam and silicon substrate, an electrostatic force pulls the beam towards the substrate. Beyond a threshold voltage called the pull-in voltage, the beam snaps down abruptly and contacts the nitride dielectric. Both Young's

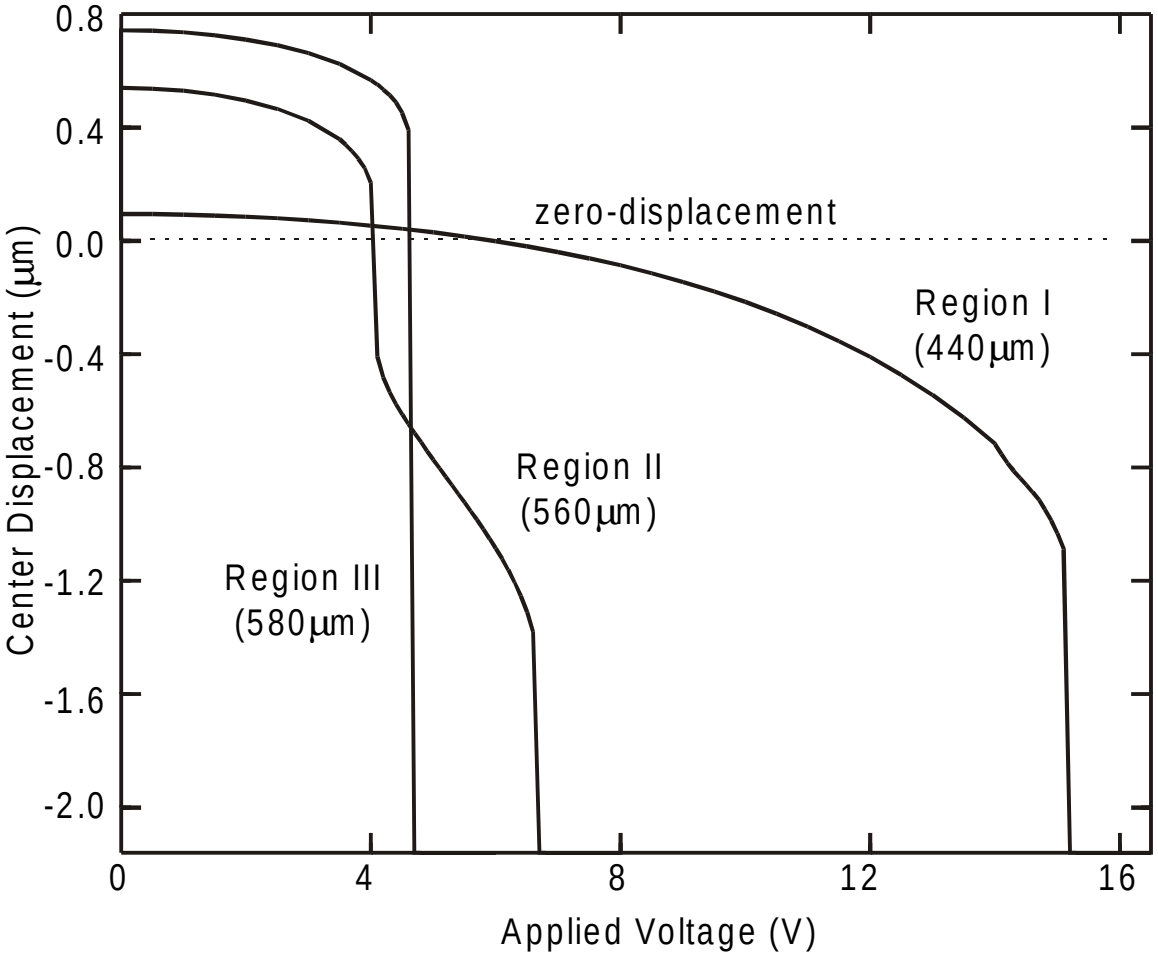

Fig. 11. *Three different types of pull-in behavior corresponding to the regions in Fig. 9.*

modulus and residual stress can be extracted by fitting simulation results to pull-in voltage measurements. An HP 4275A capacitance-voltage (CV) meter was used to apply

a bias voltage and to sense the abrupt increase in capacitance at pull-in [chan]. The stress parameter extracted from these measurements is consistent with that determined in the previous section. The extracted Young's modulus for these beams is 135GPa which is consistent with what was obtained for a previous MUMPs run [chan], and also similar to what was obtained by Sharpe [9] but somewhat lower than that obtained by Gupta [12].

Table 1: Simulation Parameters

Measured Thicknesses (μm)	
POLY0 (with gold)	0.53
POLY0 (without gold)	0.54
POLY1	1.99
Dimple depth	0.76
Sacrificial PSG	2.16
Nitride (electrical)	0.074
Stepup sidewall	1.80

Extracted Properties	
Initial biaxial stress	7.36 MPa
Young's modulus	135 GPa

The simulation fit is good with the kink at 580μm captured accurately as shown in Fig. 9 although the simulated voltages in Region III are slightly lower than those measured. The three types of pull-in behavior corresponding to the regions in Fig. 9 are shown in Fig. 11. A short beam in Region I will deflect continuously with increasing voltage until the gap decreases to about 1.0μm then snap down to the nitride dielectric. A longer beam in Region II that has an initial buckling displacement deflects continuously then snaps down to a stable state below the zero-displacement position. From there, it continues to deflect with increasing voltage before finally snapping down again, this time contacting the nitride. This two-step pull-down phenomenon does not occur for longer beams in Region III because there is no stable state below zero-displacement so the beams snap down all the way to the nitride. In contrast to beams in the first two regions, beams exhibiting this third type of behavior have pull-in voltages that increase with beam

length because the buckling amplitudes and hence the effective gaps increase with beam length. With the additional dependence of effective gap on initial stress, the pull-in voltages of these post-buckled beams are more sensitive to initial stress than the pull-in voltages of shorter beams.

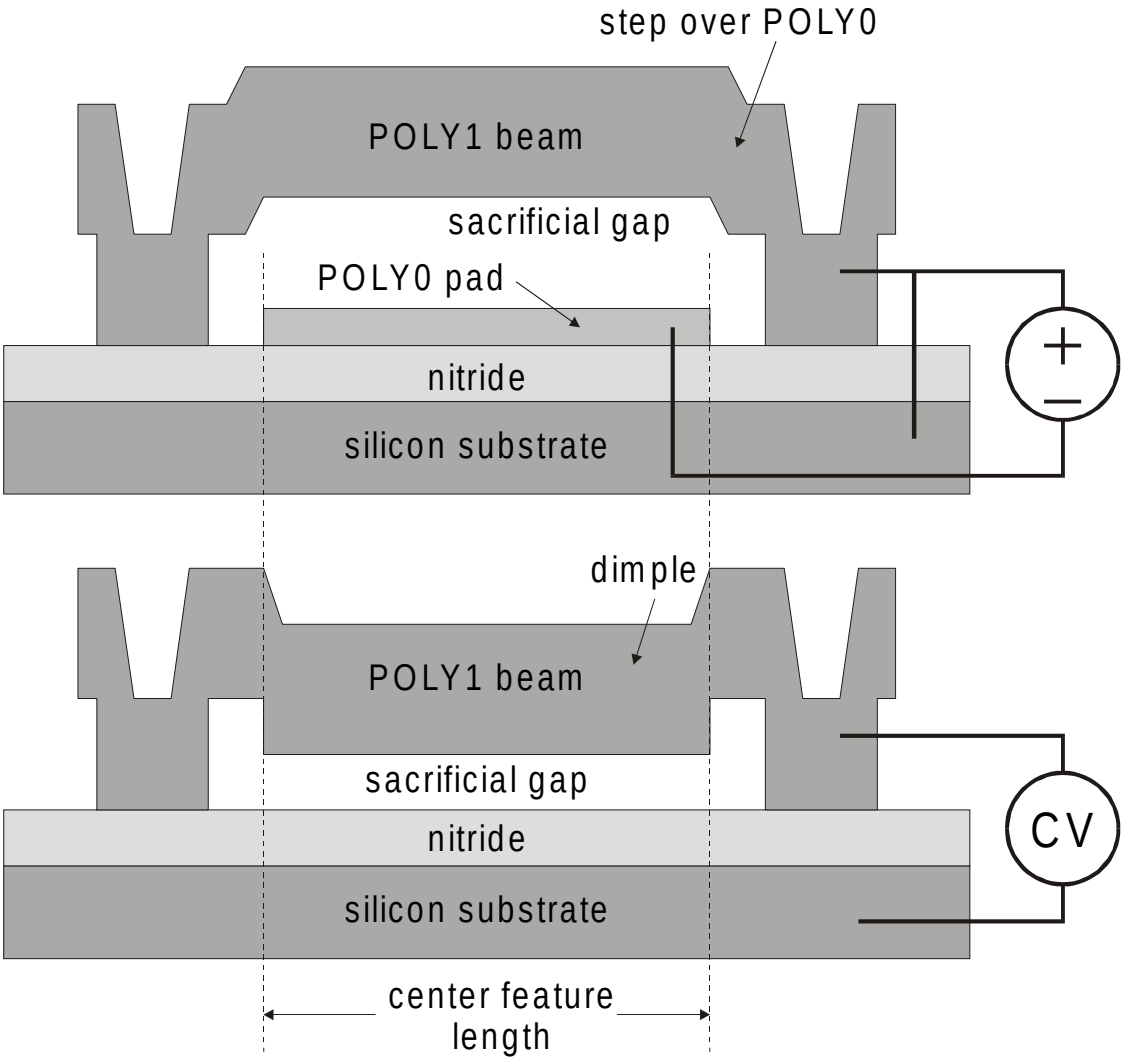

Fig. 12. *Profiles of beam with steps over POLY0 and beam with steps into dimple. The beam and silicon substrate are at the same potential for beams actuated over POLY0.*

4. Calibration of beams with multiple discontinuities

Beams fabricated out of conformal polysilicon can have dimples, and steps over underlying POLY0 layers thus requiring two additional model parameters – dimple depth

and POLY0 thickness. These parameters were measured interferometrically then included in the Abaqus model using the SEM of Fig. 8 as a guide to the actual shape of the discontinuities. The step over POLY0 is rather gradual because the conformal POLY1 is itself deposited over a conformal layer of PSG.

Fig. 12 shows test structures designed to examine the effects of these discontinuities. Once again, the pull-in voltages and buckling amplitudes of beams of various lengths were measured. The pull-in voltages of the beams with dimples were

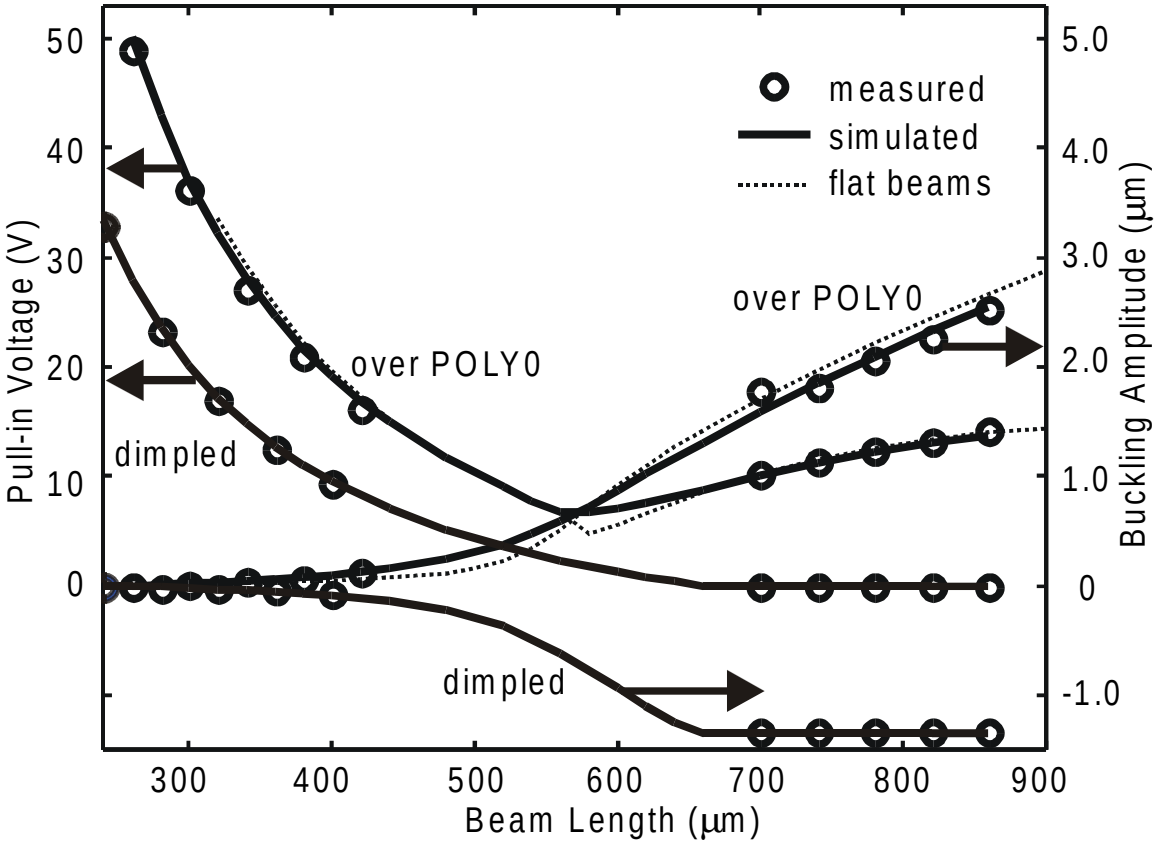

Fig. 13. *Pull-in voltages and buckling amplitudes as functions of beam length for beams over POLY0 and beams with dimples. Values for flat beams are in dotted lines.*

measured using a CV meter whereas the pull-in voltages of the beams over POLY0 were measured using an HP4155A semiconductor parameter analyzer. When pull-in occurs for beams over POLY0, direct conductor-to-conductor contact is made and DC current

will flow. This can be a destructive measurement if fusing occurs. On the other hand, pull-in can be difficult to determine if the beam discharges when it contacts the POLY0 pad and then pops back up. It is important to observe the deflection of the beam continually and note the first instance of instability indicating pull-in.

Pull-in voltage and buckling amplitude are plotted as functions of length for both beams with dimples and beams over POLY0 in Fig. 13. The beams over POLY0 behave quite similarly to flat beams. The initial sacrificial gap for these structures is 0.01μm larger than for flat beams over nitride as explained earlier. However, the total effective gap is smaller due to the absence of the nitride dielectric resulting in slightly lower pull-

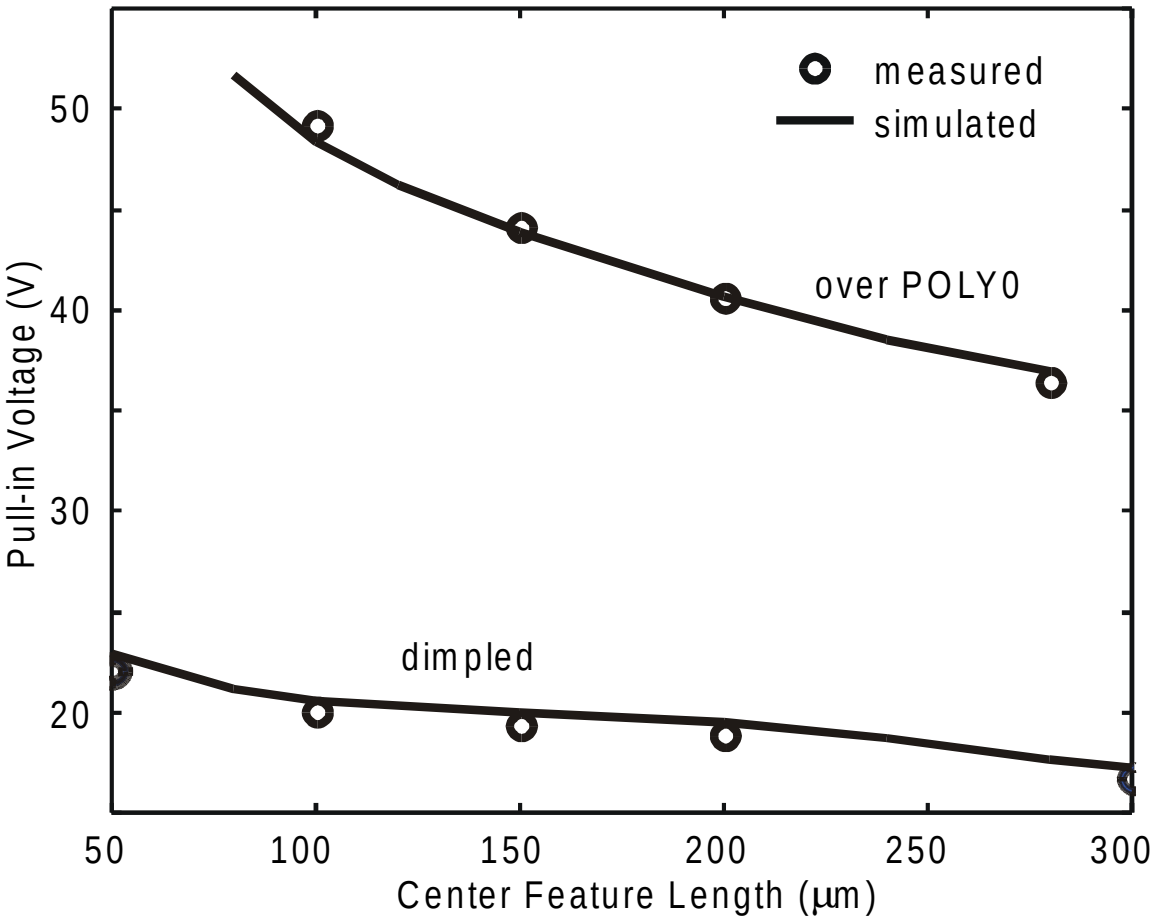

Fig. 14. *Pull-in voltages as functions of center feature length. The beam over POLY0 is 300μm long and the beam with the dimple is 320μm long.*

in voltages. The transition in buckling amplitudes from the pre-buckled to the post-buckled states is more gradual and begins earlier due to the increased compliance at the boundaries. The amplitudes are also slightly smaller. The same three regions of pull-in behavior are observed. On the other hand, the characteristics of beams with dimples deviate rather significantly from those of flat beams. The dimples cause the beams to

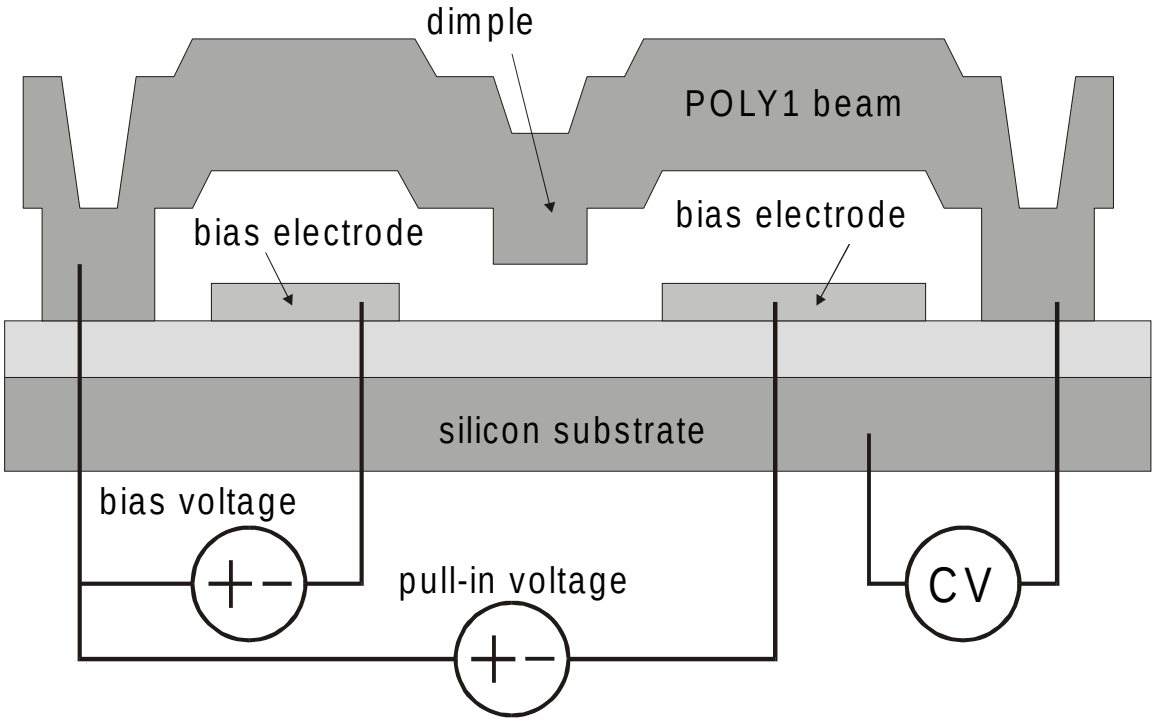

Fig. 15a. *Profile of dual-bias-electrode structure. Pull-in voltages are measured as functions of bias.*

buckle downwards systematically instead of upwards. Therefore, the post-buckled pull-in voltages do not rise with beam length but instead go to zero once the beams buckle into contact with the nitride. As for the beams over POLY0, the transition from pre-buckled to post-buckled states is more gradual and occurs earlier. The pull-in voltages are lower compared to flat beams of similar length because the effective gap is smaller by the dimple depth. The simulation fits are good, indicating that the geometrical model is valid.

Pull-in voltages of beams with shorter center features and thus with discontinuities closer to the beam center were measured to obtain the curves of Fig. 14. The pull-in voltages of beams over POLY0 increase as the POLY0 pad decreases in length. A similar trend is observed as the dimple length decreases. The good simulation fit shows that the parallel plate electrostatic approximation still holds indicating that the electrical perturbations due to these discontinuities is small.

5. Extrapolation to dual-bias-electrode structures

The simulation model characterized in the previous sections is then used to predict the behavior of more complex dual-bias-electrode structures shown in Fig. 15a. Fig. 15b is a 3D solid model of the device generated using a geometry generation program [16] that incorporates the effects of conformal deposition and sloped sidewall

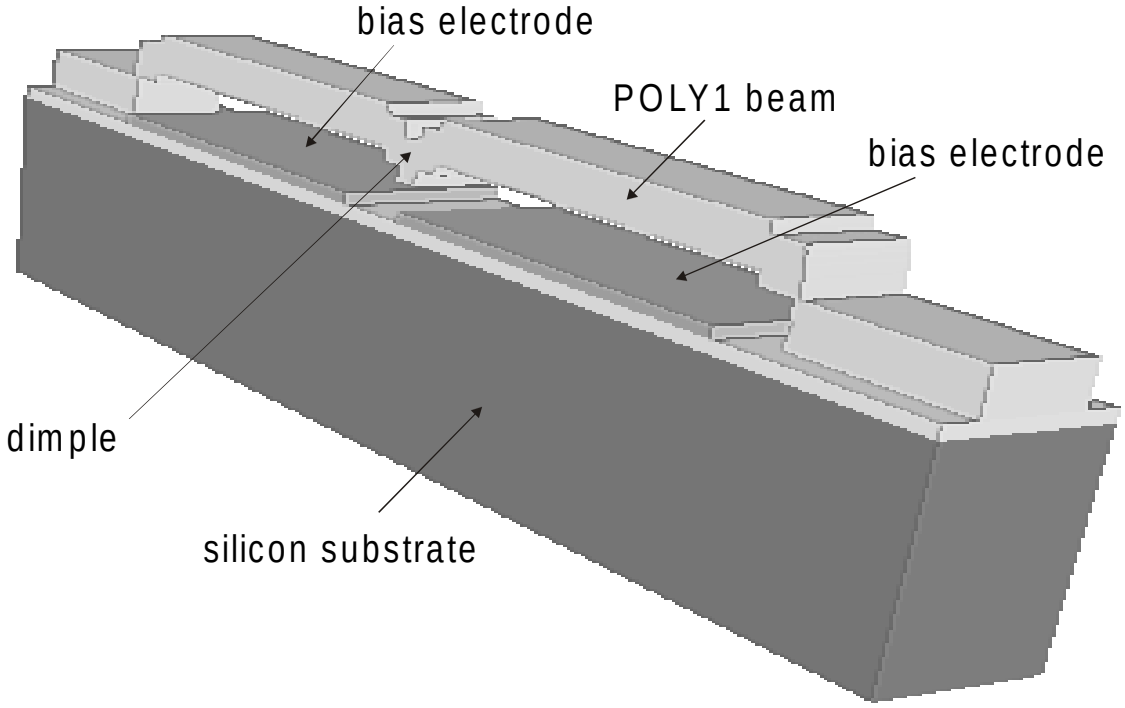

Fig. 15b. *3D solid model of dual-bias-electrode structure including effects of conformal deposition and angled etching.*

etches. The measurements of Fig. 16 are of pull-in voltages (V_{pi}) at one electrode as a function of bias voltages (V_{bias}) applied to the other electrode for three different devices. Voltages were applied using an HP4155A whereas pull-ins were sensed using a CV meter. The devices are designed such that pull-in is still abrupt despite the fact that the beam is being leveraged downwards by electrodes that are away from the beam center. These devices incorporate all the types of discontinuities characterized earlier. By having two bias electrodes, multiple precise pull-in voltage measurements can be used to characterize a single device. The dimple at the center of the beam prevents conductor-to-

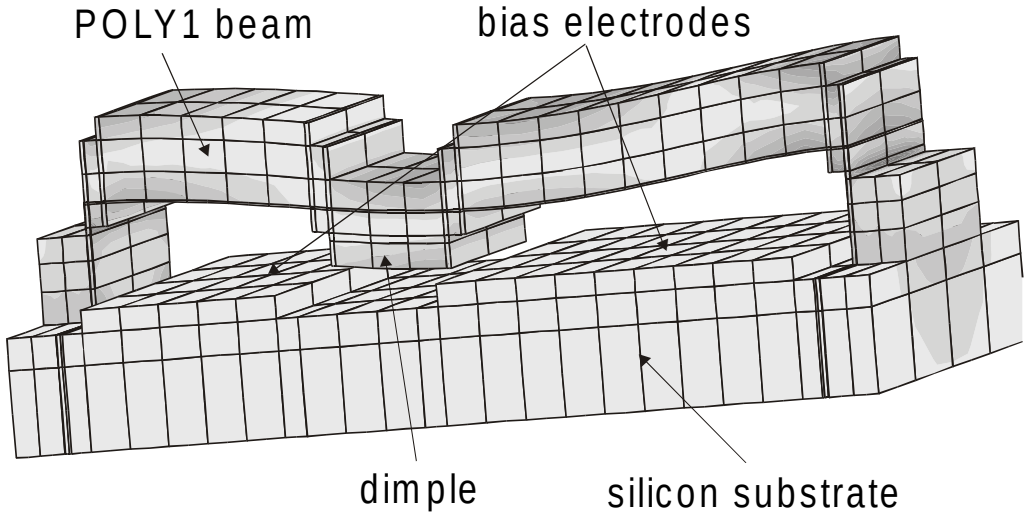

Fig. 15c. *Three-dimensional IntelliCAD model of dual-bias-electrode structure. All steps are sharp right-angles. Deformation is due to a voltage is applied to the bias electrode on the right only.*

conductor contact. Dielectric charging should not affect the measurements since there is no applied electric field between the beam and silicon substrate thus allowing consecutive measurements without the need to wait for accumulated charge to dissipate [2]. The V_{pi} vs V_{bias} curves for the devices with left and right electrodes of equal length are symmetric about the $V_{pi} = V_{bias}$ line. By swapping the bias and pull-in connections, the integrity of the devices can be verified by checking for symmetry.

The extrapolated behavior matches the measurements well. For curves such as these with segments that are primarily vertical, error norms should be calculated along the directions normal to the curves as shown in Fig. 16 rather than simply taking the

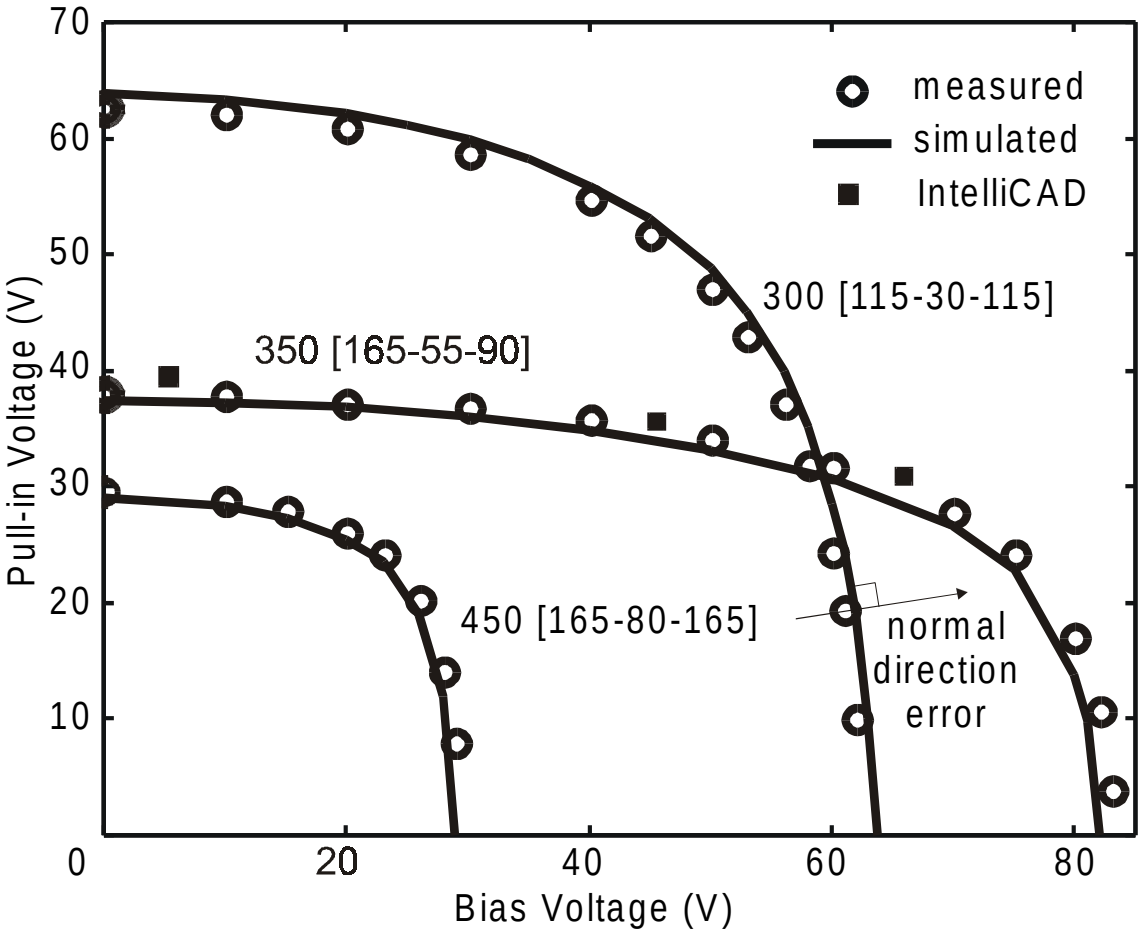

Fig. 16. *Pull-in voltage as a function of bias voltage for three dual-bias-electrode structures. The first number in the label is the beam length. In the brackets are the lengths of the pull-in electrode, dimple, and bias electrode.*

differences between the measured and simulated pull-in voltages at a particular bias voltage. Using this normal-direction error metric, the simulations match the measured values to within 3%. We have thus demonstrated that these comprehensive calibration procedures using simple test structures produce simulation model parameters that predict the behavior of more complex devices very accurately. Therefore, the model parameters

in Table 1 along with the measurement data in Fig. 16 can serve as verification test cases to evaluate the accuracy of coupled electromechanical simulators.

With those model parameters, we ran full 3D simulations using the commercial electromechanical simulator IntelliCAD. The geometry shown in Fig. 15c generated automatically by the software, however, has sharp, right-angled steps instead of smooth, rounded steps. The simulated pull-in voltages using this coarse model are slightly higher than those measured as shown in Fig. 16.

6. Conclusions

A comprehensive methodology to calibrate a simulation model to the MUMPs process of MCNC has been presented. Interferometric measurements, SEMs and electrical measurements of simple test structures along with detailed electromechanical simulations were used to extract material and geometrical parameters especially pertinent to electrostatically-actuated beams. The limits of the calibration procedure due to width-dependent variations and the effects of gold pads were discussed. The extrapolations of the simulation model to more complex devices were excellent demonstrating the viability of the dual-bias-electrode structures to serve as canonical benchmarks for coupled electromechanical simulators. Further work is necessary to uncover and characterize unanticipated non-uniformities among ostensibly similar structures, especially for cantilevers that are much more sensitive to stress gradient variations than fixed-fixed beams.

Acknowledgements

The authors would like to thank B. K. Eplett for help with the SEMs. This work was supported by the DARPA Composite CAD program (contract #F30602-96-2-0308-P00001).

References

[1] Hibbitt, Karlsson and Sorensen, Inc., ABAQUS/Standard User's Manual, version 5.6, Pawtucket, 1996.

[2] E. K. Chan, K. Garikipati, R.W. Dutton, "Characterization of contact electromechanics through capacitance-voltage measurements and simulations," to appear in *Journal of Microelectromechanical Systems*, Mar/Jun 1999.

[3] IntelliSense Corp., IntelliCAD 98 User's Manual, Wilmington, 1998.

[4] Microcosm Corp., MEMCAD User's Manual, v4, Cambridge, 1998.

[5] K. E. Petersen, "Dynamic micromechanics on silicon: Techniques and devices," *IEEE Transactions of Electron Devices*, ED-25, pp. 1241-1250, 1978.

[6] H. Guckel, T. Randazzo, D. W. Burns, "A simple technique for the determination of mechanical strain in thin films with applications to polysilicon," *Journal of Applied Physics*, 57 (5), pp. 1671-1675, Mar 1985.

[7] T. P. Weihs, S. Hong, J. C. Bravman, W. D. Nix, "Mechanical deflection of cantilever microbeams: A new technique for testing the mechanical properties of thin films," *Journal of Materials Research*, 3 (5), pp. 931-942, Sep/Oct 1988.

[8] K. Najafi, K. Suzuki, “Measurement of fracture stress, Young’s modulus, and intrinsic stress of heavily boron-doped silicon microstructures,” *Thin Solid Films*, vol. 181, pp. 251-258, Dec 1989.

[9] W. N. Sharpe, Jr., K. Turner, R. L. Edwards, “Measurements of the effect of specimen size on Young’s modulus and tensile strength of polysilicon,” *in Late News Poster Session Supplemental Digest of IEEE Solid State Sensor and Actuator Workshop*, Hilton Head, pp. 17-19, Jun 1998.

[10] D. A. Koester, R. Mahadevan, A. Shishkoff, K. W. Markus, SmartMUMPs Design Handbook including MUMPs Introduction and Design Rules (rev. 4), Microelectronics Center of North Carolina, Jul 1996.

[11] J. C. Marshall, D. T. Read, M. Gaitan, “Analysis of fixed-fixed beam test structures,” in *Proceedings of SPIE Conference on Microlithography and Metrology in Micromachining II*, Austin, TX, vol. 2880, pp. 46-55, Oct 1996.

[12] R. K. Gupta, “Electrostatic pull-in test structure design for in-situ mechanical property measurements of microelectromechanical systems (MEMS),” Ph.D. thesis, Massachusetts Institute of Technology, USA, Jun 1997.

[13] W. Fang, J. A. Wickert, “Post-buckling of micromachined beams,” *Journal of Micromechanics and Microengineering*, Vol. 4 no. 3, pp. 116-122, Sep 1994.

[14] J. C. Marshall, MUMPs Users’ Group Meeting, Santa Clara, Sep 1998.

[15] J. J.-Y. Gill, L. V. Ngo, P. R. Nelson, C.-J. Kim, “Elimination of extra spring effect at the step-up anchor of surface micromachined structure,” *Journal of Microelectromechanical Systems*, vol. 7., no. 1, pp. 114-121, Mar 1998.

[16] N. M. Wilson, R. W. Dutton, P. M. Pinsky, “Utilizing existing TCAD simulation tools to create solid models for the simulation-based design of MEMS devices,” *Proceedings of ASME International Mechanical Engineering Congress and Exposition*, Anaheim, DSC-Vol. 66, pp. 565-570, Nov 1998.